Nanoscale

Tannic acid-inspired star polymers for functional metal-phenolic networks with tunable pore sizes

Journal:	*Nanoscale*
Manuscript ID	NR-COM-05-2022-002682.R1
Article Type:	Communication
Date Submitted by the Author:	10-Sep-2022
Complete List of Authors:	Cheng, Bohan; The University of Tokyo, Department of Materials Engineering Lu, Sifan; The University of Tokyo, Department of Materials Engineering Liao, Wenting; The University of Tokyo, Department of Materials Engineering Wang, Chenyu; The University of Tokyo, Department of Materials Engineering Richardson, Joseph; The University of Tokyo, Department of Materials Engineering Ejima, Hirotaka; The University of Tokyo, Department of Materials Engineering

COMMUNICATION

Tannic acid-inspired star polymers for functional metal-phenolic networks with tunable pore sizes

Received 00th January 20xx,
Accepted 00th January 20xx

DOI: 10.1039/x0xx00000x

Bohan Cheng,[a] Sifan Lu, [a] Wenting Liao, [a] Chenyu Wang, [a] Joseph J. Richardson [a] and Hirotaka Ejima*[a]

Tannic acid (TA) is a structurally undefined natural dendritic polyphenol. Here, we introduce a series of TA-inspired polymers with different arm lengths, M_n, and phenolic groups that can be used to engineer metal-phenolic network (MPN) capsules with different properties including controlled permeability, high biocompatibility, and fluorescence.

Among the various phenolic compounds found in nature, tannic acid (TA) is of particular interest to materials science, due to its ability to form functional materials used in various applications including biomedicine,[1,2] environmental remediation,[3,4] and adhesion.[5–7] The functionality of TA is tied to its unique 5-arm topology with multiple phenolic units running along each arm. This dendritic structure allows for TA to interact with itself and other molecules and substrates via hydrogen bonding, electrostatic interactions, hydrophobic interactions, metal coordination, and π-π stacking.[8] In nature, TA is a mixture of polygalloyl glucoses or polygalloyl quinic acid esters with different numbers of phenolic groups per arm, but the empirical formula of TA is generally given as $C_{76}H_{52}O_{46}$.[9] Although TA has a variety of superior properties, the uncertain stoichiometry, coupled with the dynamic composition (hydrolysis and condensation) in natural and synthetic TA hinders fundamental investigations into the structure-function relationship of TA and TA-based materials.

TA is one of the most widely used phenolic ligands for constructing nanomaterials including metal-phenolic networks (MPNs)[10] with promising biomedical applications[11–14]. MPN thin films can be constructed on substrates of different size, shape, and composition due to the high adhesion of phenolic molecules to surfaces,[15–17] where the metal ions cross-link and stabilize the film. Moreover, by coating sacrificial templates, hollow capsules that useful for biotechnology can be formed after template removal.[18–21] Pore sizes of MPN capsules can be controlled by careful choice of the pH, ligands, and type of metal ions used.[22,23] However, fundamental questions still remain on how the ligand architecture effects the physicochemical properties of the films and the resulting pores of MPN capsules. Herein, we report a series of star-shaped phenolic polymers that mimic the composition and topology of TA while maintaining a carbon backbone, which we term "tannic acid-inspired polymers" (TIPs). Using a newly reported glucose-based initiator for nitroxide mediated polymerization (NMP), the molecular weight (M_n) and unit composition (gallol vs catechol number) of the TIPs could be controlled by the feed ratio of catechol/gallol monomers and reaction time, and other functional units could be incorporated during synthesis. The TIP-based MPNs had tunable permeability based on both their M_n and their unit composition, and demonstrated similar biocompatibility to natural TA-based MPNs. Overall, TIPs are straightforward to synthesize, and offer promise for making functional phenolic materials.

To mimic the phenolic groups in TA, monomers bearing either protected catechol (3,4-di(methoxymethoxy)styrene, DMMS) or gallol moieties (3,4,5-tri(methoxymethoxy)styrene, TMMS) were synthesized using a protocol previously reported by our group.[24,25] The glucose initiator was synthesized in two steps to mimic the glucose core of TA. In the first step, D(+)-glucose was reacted with 2-bromoisobutyryl bromide to get the ATRP initiator Glu-Br_5 according to previous reports.[26,27] However, Glu-Br_5 cannot directly polymerize TMMS and DMMS because of the poor reactivity of the ATRP system when electron-donating groups including $-OCH_3$ and methoxymethyl ether (MOM) substitute the 3, 4 or 5 positions of styrene units.[28–30] Also, metals and acids[31,32] that may be commonly used in ATRP systems would cause the deprotection of the monomers during the polymerization process, where the exposed phenols could then quench the radicals necessary for chain propagation.[33] In order to avoid these issues, the Glu-Br_5 was further modified to alkoxyamine Glu-$TEMPO_5$ for NMP[34] via the copper-catalyzed atom transfer radical addition process.[35] TIPs were then synthesized by the one-pot polymerization of DMMS, TMMS, and Glu-$TEMPO_5$ which was followed by a deprotection process using dilute HCl (0.1 M).

The synthetic flowchart for preparing TIPs from glucose is illustrated in Fig. 1a, and ^{1}H-NMR and ^{13}C-NMR were used to confirm each intermediary (Fig. S1–S16 and Table S1). The successful synthesis of Glu-$TEMPO_5$ was also confirmed by high-resolution mass spectrometry (HRMS). By changing the feed amounts of monomers and initiator, TIPs with different M_n and catechol/gallol ratios can be synthesized. The "living" properties of NMP for DMMS and TMMS were evidenced by first order kinetic plots for the polymerization of

[a] Department of Materials Engineering, The University of Tokyo, 7-3-1 Hongo, Bunkyo-ku, Tokyo 113-8656, Japan.
Electronic Supplementary Information (ESI) available: [details of any supplementary information available should be included here]. See DOI: 10.1039/x0xx00000x

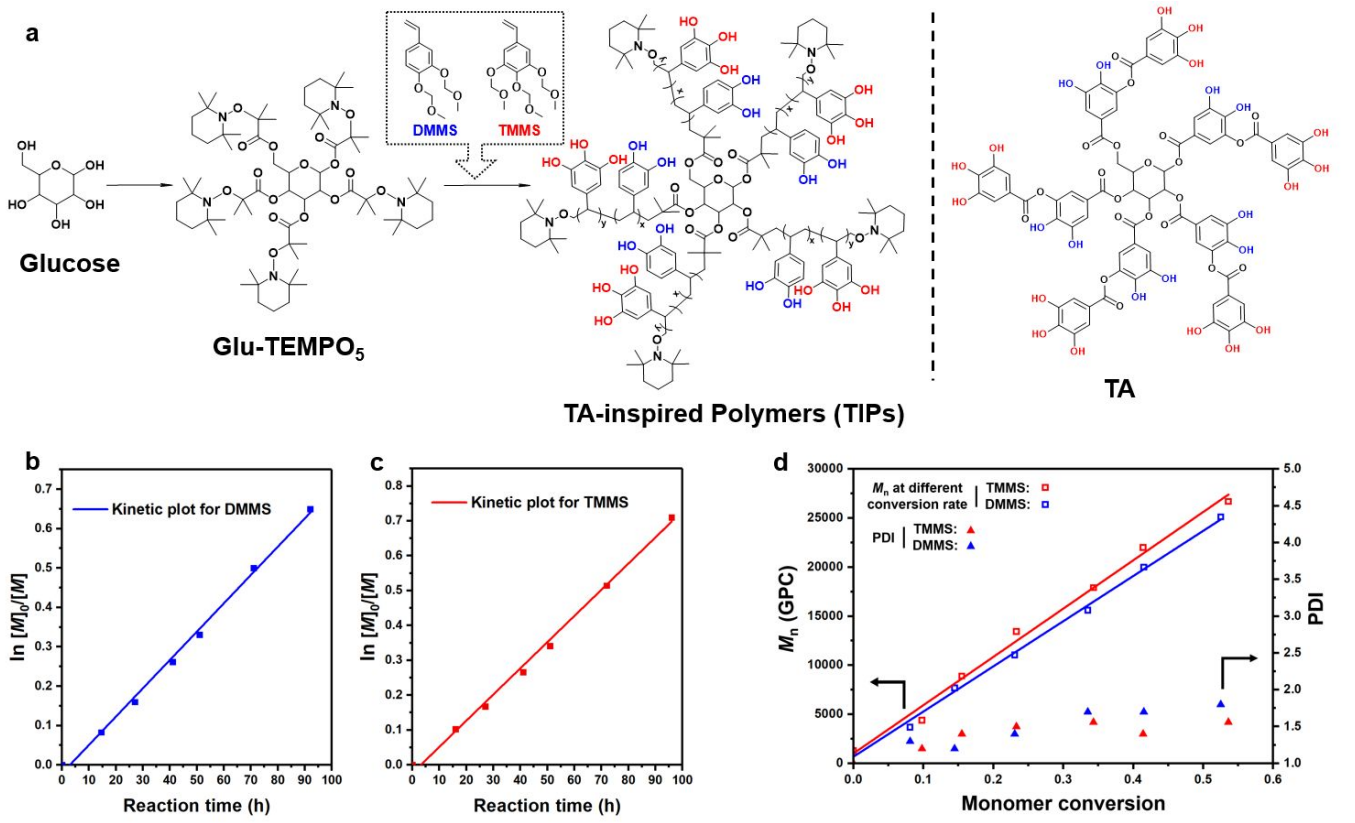

Fig. 1 Synthesis of TIPs. (a) Flowchart of TIP synthesis from the glucose-core and the reference structure of TA. (b) First order polymerization kinetic plot of DMMS with Glu-TEMPO$_5$. (c) First order polymerization kinetic plot of TMMS with Glu-TEMPO5. (d) Evolution of M_ns with conversions for the polymerizations of DMMS (blue) and TMMS (red) with Glu-TEMPO$_5$.

DMMS and TMMS (Fig. 1b and 1c). Monomers were polymerized in anisole at 130 °C for different periods of time with the [Monomer]:[Initiator] set at 3000:1. Fig. 1d shows the evolution of M_n with conversions for the polymerizations of DMMS and TMMS as well as their PDIs, indicating that NMP initiator Glu-TEMPO$_5$ can effectively polymerize DMMS and TMMS.

The catechol/gallol ratios were 1:0, 1:1, 1:2, 2:1, and 0:1 (See Table S1 for full details) for the different synthesized TIPs, and for each ratio, three M_ns were synthesized, namely 3–4 kDa, 6–7 kDa, and 10–12 kDa. Because the gel permeation chromatography (GPC) results were obtained before removing the MOM protection groups, the 3–4 kDa TIPs have similar numbers of phenolic units to idealized TA (1.7 kDa), with 1 catechol and 1 gallol unit per arm. TIPs at 6–7 kDa and 10–12 kDa are higher than idealized TA, and for example, the TIP with a 1:1 catechol/gallol ratio at 12 kDa would have 4 catechol units and 4 gallol units on each arm. MPN coating performance of TIP (catechol/gallol=2:1, 3-4 kDa) on flat surfaces was confirmed using a quartz crystal microbalance (QCM) (See ESI for experimental details). As a result, TIP-based MPN coatings showed material independency and the coating amounts are higher than conventional TA-based MPN coatings (Fig. S17).

Hollow TIP-based MPN capsules were then prepared by mixing the TIPs (5 µL, 40 mg/mL in ethanol) with Fe^{3+} ions ($FeCl_3{\cdot}6H_2O$, 5 µL, 6.5 mg/mL in DI-water). Coating was performed via repeating the addition of TIPs and Fe^{3+} ions three times before removal of the spherical polystyrene templates (Fig. S18, see ESI for experimental details) by THF to obtain $(Fe^{3+}/TIP)_3$ hollow capsules. The shapes and dispersity of the capsules were confirmed by optical microscopy. To determine the importance of the star nature of the TIPs (and TA indirectly), linear catechol/gallol polymers (LPs) with different ratios were also used to prepare $(Fe^{3+}/LP)_3$ capsules (Fig. S19). Importantly, all $(Fe^{3+}/TIP)_3$ except for the catechol-only TIP could readily form robust capsules, while the $(Fe^{3+}/LP)_3$ could only produce fragile and broken capsules in the conditions used in this study. These results indicate that the non-linear topology of TA and TIPs has a positive effect on robust interconnected networks. For TIPs that only contained catechol units, severely aggregated was observed, likely due to the poor water solubility of catecholic TIPs. In fact, the solubility of the gallol-only TIPs (5.0 mg/mL in water) is 20 times higher than the catechol-only TIPs (0.25 mg/mL in water). This not only demonstrates the importance of the gallol units in natural TA, but also highlights that the solubility of synthetic phenolics is easily controllable and can be tuned depending on the application of interest.

The $(Fe^{3+}/TIP)_3$ capsules had an LMCT band between 500 and 700 nm using UV-VIS spectroscopy, with the band appearing above pH 4 (Fig. S20). Importantly, $(Fe^{3+}/TIP)_3$ thin films did not pose any observable toxicity to mouse fibroblast cells L929 (Fig. S21, see SI for experimental details), suggesting that Fe^{3+}/TIP MPNs have similar biocompatibility to conventional MPNs formed from Fe^{3+} and natural TA.

An important property of MPNs specifically, is their permeability. Therefore, the permeability of $(Fe^{3+}/TIP)_3$ capsules prepared from different TIPs was examined using FITC-labeled dextran fluorescent probes of six different molecular weights. The radius of gyration of the fluorescent probes relates to their size, and

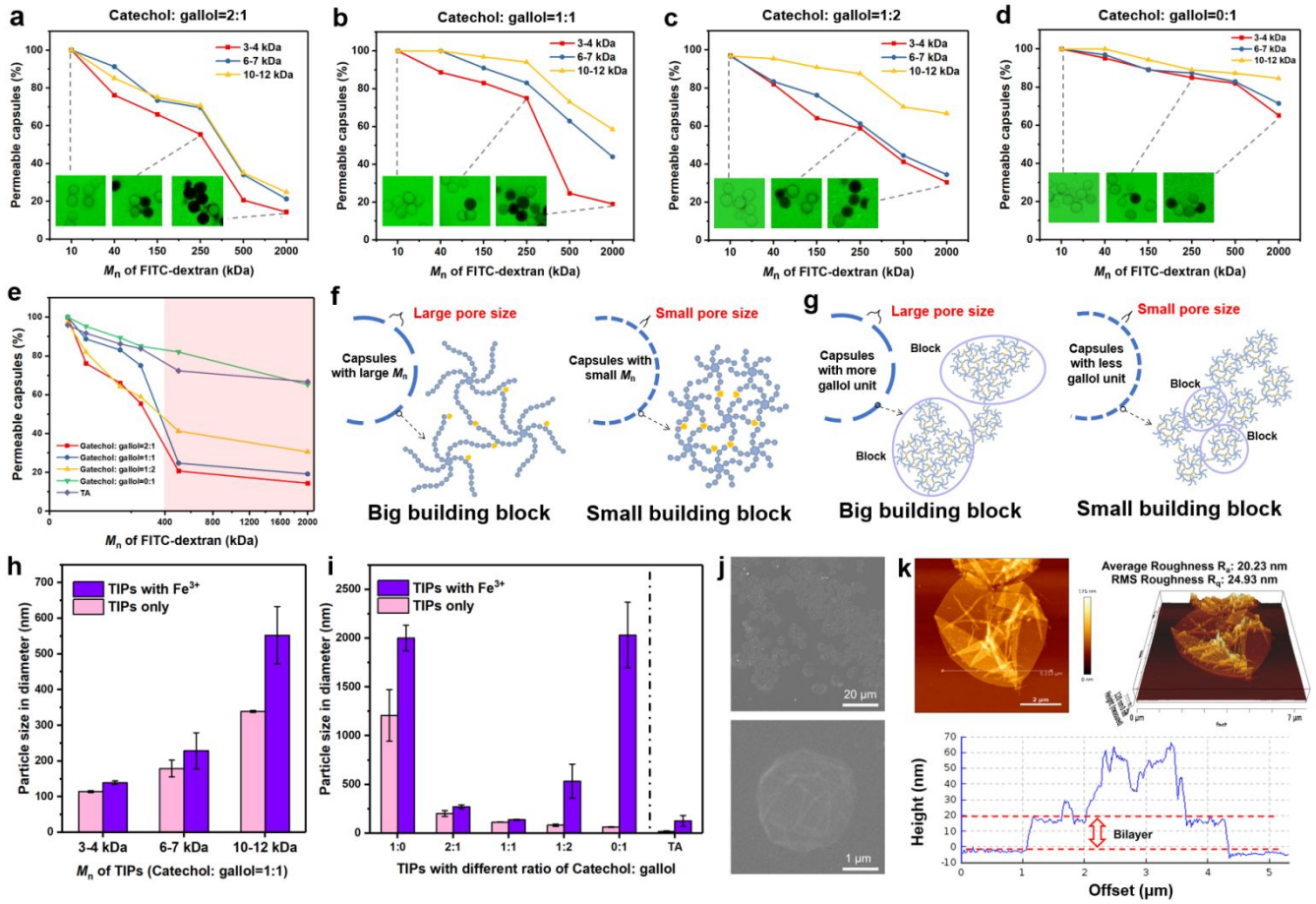

Fig. 2 Permeabilities of $(Fe^{3+}/TIP)_3$ hollow capsules. (a–d) Permeabilities of TIPs with different M_n. The catechol/gallol ratio was set from 2:1 to 0:1. (e) Permeabilities of TIPs with different phenolic compositions. The M_n was set at 3–4 kDa. (f) The mechanism of different permeabilities shown in TIPs with low and high M_n. (g) The mechanism of different permeabilities shown in TIPs with different gallol unit compositions. (h) Size of conjugations of 1:1 TIP with different M_n. (i) Size of conjugations of TIP with different phenolic compositions. The M_n was set at 3–4 kDa. (j) Typical SEM picture of capsules (2:1, 3–4 kDa). (k) Representative AFM picture of capsules (2:1, 3–4 kDa) and the bilayer thickness of a capsule.

therefore they are regularly used to monitor the permeability of capsules. Fluorescent cross-sectional images of the capsules were taken using confocal laser scanning microscopy (CLSM) within 15 min of incubating the capsules with FITC-dextran (See ESI for experimental details). Generally, the permeability of the capsules increased when the M_n (Fig. 2a–d) of the TIPs increased. TIPs with a catechol/gallol ratio of 2:1 (Fig. 2a) formed the most impermeable capsules, as capsules with higher gallol ratios were generally more permeable (Fig. 2e). For example, when the M_n was 3–4 kDa, the 2:1 ratio capsules were only about 13% permeable to 2,000 kDa FITC-dextran. The most permeable capsule was the 0:1 ratio capsule (gallol only) with the high M_n, which is almost 90% permeable to 2,000 kDa FITC-dextran.

Taken together, the unit composition and M_n can influence the permeability of capsules, and the topology additionally effects the robustness of the capsules. These parameters for controlling the permeability of capsules are explained in Fig. 2f and 2g, and have not been reported in previous studies, but allow for similar control as previous reports on tuning the permeability of (Fe^{3+}/TA) capsules using other parameters, such as pH.[22] Briefly, TIPs with higher M_n had longer arms, and the steric hindrance of the long polymer chains lead to a looser network with larger defects. Dynamic light scattering (DLS) was used to characterize the size of 1:1 TIPs with different M_n before and after their coordination with Fe^{3+} (Fig. 2h). As a result, the unit size of 1:1 TIP at 3–4 kDa was around 100 nm before coordination and 140 nm after coordination, while the 1:1 TIP with higher M_n had larger unit size (350–600 nm).

On the other hand, gallol units are known to have stronger crosslinking abilities than catechol units because of the additional hydroxy group, and TIPs with more gallol units tended to form bigger building blocks, which was supported by DLS results (Fig. 2i) and microscope images (Fig. S22). As the composition of gallol units increased, the size of the unit decreased (from ~2000 nm to ~140 nm) until the catechol:gallol ratio came to 1:1. This decrease is likely due to the poor water solubility of catechol-dominated TIPs themselves. Further increasing the ratio of gallol units until gallol-only TIPs were reached, led to a significant increase in unit size (from ~140 nm to ~2200 nm). Energy dispersive X-ray spectroscopy (EDS) showed that with the increase of gallol composition from catechol:gallol 2:1 to 1:2, the elemental composition of Fe increased from 2.01% to 2.67%, indicating more Fe^{3+} ions were incorporated in units of gallol-domained TIPs (Table S2). These units themselves could be dense and impenetrable, but the space between the units would become bigger. Scanning electron microscopy (SEM) and atomic force microscopes (AFM), of representative capsules demonstrated collapsed capsules with the typical folds of dry MPN

capsules (Fig. 2j and k). The thickness of capsules was roughly 13 nm (Fig. 2k and Table S3), which is similar to conventional MPNs formed from Fe^{3+} and natural TA, and indicated that the permeability differences were not thickness-dependent.[15,22]

Interestingly, conventional $(Fe^{3+}/TA)_3$ capsules had similar permeability (~66% permeable) to the synthetic pure gallol $(Fe^{3+}/TIP)_3$ capsules. The reason may be due to different metal/ligand concentrations and different polymer backbones, and moreover the density of hydroxy groups in TIPs were lower than that in TA. This result indicates the polymer backbone can also influence the properties of MPNs.

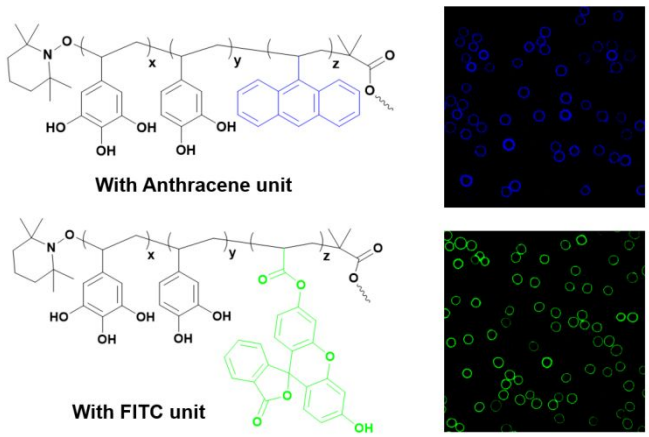

Fig. 3 Introduction of different functionalities to capsules by one-pot copolymerization.

Importantly, the synthesis of the TIPs allowed for the incorporation of other functionalities simply by the addition of other monomers during synthesis (Fig. 3). Specifically, two different model molecules, namely fluorescein monomers (fluorescein o-acrylate (green) and 9-Vinylanthracene (deep blue)) were separately copolymerized with TMMS and DMMS in one pot. By introducing 5% fluorescein units into the TIPs, $(Fe^{3+}/TIP)_3$ capsules with different colors could readily be prepared, which demonstrates the versatility of TIPs and the de novo synthesis of phenolic molecules. For example, targeting ligands, click groups, therapeutics, or various other functional molecules could easily be incorporated into the TIPs during synthesis in the future to target various applications.

Conclusions

In conclusion, a series of TIPs were synthesized to mimic the structure and molecular functionality of the natural polyphenol, TA. The physicochemical properties of MPN coatings prepared from these TIPs were examined using hollow capsules, and the $(Fe^{3+}/TIP)_3$ capsules had programable permeability, where higher M_n and higher gallol compositions led to capsules with higher permeability. The biocompatibility and the ability to incorporate other functional molecules in the TIPs and resultant capsules were all demonstrated, thereby revealing the great potential of these new synthetic phenolic polymers. We foresee that this synthesis strategy will generate numerous “tips” for the MPN and thin film fields for elucidating fundamentals underpinning phenolic materials, while also allowing for breakthroughs in various applications.

Author Contributions

Bohan Cheng: Conceptualization, Investigation, Data Curation, Writing-Original Draft, Writing-Reviewing and Editing. Sifan Lu: Investigation, Visualization. Wenting Liao: Investigation. Chenyu Wang: Investigation. Joseph J. Richardson: Investigation, Data Curation, Writing-Reviewing and Editing. Hirotaka Ejima: Conceptualization, Validation, Supervision, Writing-Reviewing and Editing, Project administration. All authors have given approval to the final version of the manuscript.

Conflicts of interest

There are no conflicts to declare

Acknowledgement

This research was partially supported by the Japan Society for the Promotion of Science (JSPS) KAKENHI (Grant No. 20F20373, 20H02581 and 20K20641) and Japan Science and Technology Agency (JST) through the Precursory Research for Embryonic Science and Technology (PRESTO) grant number JPMJPR21N4. H.E. acknowledges Katsu Research Encouragement Award of the University of Tokyo and MEXT Leading Initiative for Excellent Young Researchers. J.J.R. acknowledges JSPS for the postdoctoral fellowship for research in Japan (P20373). This work was performed in part at One-stop Sharing Facility Center for Future Drug Discoveries in Graduate School of Pharmaceutical Sciences, the University of Tokyo.

Notes and references

1 J. Guo, Y. Ping, H. Ejima, K. Alt, M. Meissner, J. J. Richardson, Y. Yan, K. Peter, D. von Elverfeldt, C. E. Hagemeyer and F. Caruso, *Angew. Chem. Int. Ed.*, 2014, **53**, 5546–5551.

2 Y. Guo, X. Zhang, W. Sun, H.-R. Jia, Y.-X. Zhu, X. Zhang, N. Zhou and F.-G. Wu, *Chem. Mater.*, 2019, **31**, 10071–10084.

3 C. Dong, Z. Wang, J. Wu, Y. Wang, J. Wang and S. Wang, *Desalination*, 2017, **401**, 32–41.

4 W. Yan, L. Liu, C. Dong, S. Xie, X. Zhao and C. Gao, *Desalination*, 2021, **498**, 114639.

5 B. Li, J. J. Whalen, M. S. Humayun and M. E. Thompson, *Adv. Funct. Mater.*, 2020, **30**, 1907478.

6 J. Guo, W. Sun, J. P. Kim, X. Lu, Q. Li, M. Lin, O. Mrowczynski, E. B. Rizk, J. Cheng, G. Qian and J. Yang, *Acta Biomater.*, 2018, **72**, 35–44.

7 Y. Xu, R. Rothe, D. Voigt, S. Hauser, M. Cui, T. Miyagawa, M. Patino Gaillez, T. Kurth, M. Bornhäuser, J. Pietzsch and Y. Zhang, *Nat. Commun.*, 2021, **12**, 2407.

8 W. Yan, M. Shi, C. Dong, L. Liu and C. Gao, *Adv. Colloid Interface Sci.*, 2020, **284**, 102267.

9 E. Fischer, *J. Am. Chem. Soc.*, 1914, **36**, 1170–1201.

10 H. Ejima, J. J. Richardson and F. Caruso, *Nano Today*, 2017, **12**, 136–148.

11 J. H. Park, K. Kim, J. Lee, J. Y. Choi and D. Hong, *Angew. Chem. Int. Ed.*, 2014, **53**, 12420–12425.
12 G. Fan, P. Wasuwanich, M. R. Rodriguez-Otero and A. L. Furst, *J. Am. Chem. Soc.*, 2022, **144**, 6, 2438–2443.
13 J. Zhou, Z. Lin, Y. Ju, M. A. Rahim, J. J. Richardson and F. Caruso, *Acc. Chem. Res.*, 2020, **53**, 1269–1278.
14 D. Wu, J. Zhou, M. N. Creyer, W. Yim, Z. Chen, P. B. Messersmith and J. V Jokerst, *Chem. Soc. Rev.*, 2021, **50**, 4432–4483.
15 H. Ejima, J. J. Richardson, K. Liang, J. P. Best, M. P. van Koeverden, G. K. Such, J. Cui and F. Caruso, *Science*, 2013, **341**, 154–157.
16 H. Lee, J. Park, S. Y. Han, S. Han, W. Youn, H. Choi, G. Yun and I. S. Choi, *Chem. Commun.*, 2020, **56**, 13748–13751.
17 J. Lee, H. Cho, J. Choi, D. Kim, D. Hong, J. H. Park, S. H. Yang and I. S. Choi, *Nanoscale*, 2015, **7**, 18918–18922.
18 J. Guo, H. Sun, K. Alt, B. L. Tardy, J. J. Richardson, T. Suma, H. Ejima, J. Cui, C. E. Hagemeyer and F. Caruso, *Adv. Healthc. Mater.*, 2015, **4**, 1796–1801.
19 Y. Ping, J. Guo, H. Ejima, X. Chen, J. J. Richardson, H. Sun and F. Caruso, *Small*, 2015, **11**, 2032–2036.
20 P. Liu, X. Shi, S. Zhong, Y. Peng, Y. Qi, J. Ding and W. Zhou, *Biomater. Sci.*, 2021, **9**, 2825–2849.
21 J. Zhou, M. Xu, Z. Jin, R. M. Borum, N. Avakyan, Y. Cheng, W. Yim, T. He, J. Zhou, Z. Wu, Y. Mantri and J. V Jokerst, *Angew. Chem. Int. Ed.*, 2021, **60**, 26357–26362.
22 J. Chen, S. Pan, J. Zhou, Q.-Z. Zhong, Y. Qu, J. J. Richardson and F. Caruso, *Chem. Mater.*, 2020, **32**, 6975–6982.
23 C.-J. Kim, F. Ercole, Y. Ju, S. Pan, J. Chen, Y. Qu, J. F. Quinn and F. Caruso, *Chem. Mater.*, 2021, **33**, 8477–8488.
24 K. Zhan, C. Kim, K. Sung, H. Ejima and N. Yoshie, *Biomacromolecules*, 2017, **18**, 2959–2966.
25 J. Yu, B. Cheng and H. Ejima, *J. Mater. Chem. B*, 2020, **8**, 6798–6801.
26 D. M. Haddleton, R. Edmonds, A. M. Heming, E. J. Kelly and D. Kukulj, *New J. Chem.*, 1999, **23**, 477–479.
27 P. Chmielarz, *Polymer*, 2016, **102**, 192–198.
28 J. Qiu and K. Matyjaszewski, *Macromolecules*, 1997, **30**, 5643–5648.
29 S. Saha and G. L. Baker, *Appl. Surf. Sci.*, 2015, **359**, 911–916.
30 X.-Y. Wang, Z.-H. Chen, X.-L. Sun and Y. Tang, *Polymer*, 2019, **178**, 121630.
31 K. T. Reddy, R. Sreenivasulu, I. Hatti, K. Anitha and R. R. Raju, *Curr. Org. Synth.*, 2015, **12**, 67–70.
32 K. Min, H. Gao and K. Matyjaszewski, *Macromolecules*, 2007, **40**, 1789–1791.
33 K. Zhan, H. Ejima and N. Yoshie, *ACS Sustain. Chem. Eng.*, 2016, **4**, 3857–3863.
34 H. R. Lamontagne and B. H. Lessard, *ACS Appl. Polym. Mater.*, 2020, **2**, 5327–5344.
35 K. Matyjaszewski, B. E. Woodworth, X. Zhang, S. G. Gaynor and Z. Metzner, *Macromolecules*, 1998, **31**, 5955–5957.